SS, there exists a unique solution of equivalent dynamics and the SM obtained from these methods are the same. However, with boundary layers control, the SM only exists when the fast-scale dynamics is stable. The mathematical proof of this concept has already been developed earlier in multi-scale HDSs [20]. Since the power electronics converters come under this class of systems [21], [22], [23], the equivalent equation of motion derived from Utkin theory may not be successful always in predicting the existence of a unique solution [20]. It can only be successfully used when the long-time averaging of *fast-scale* oscillations become zero, in other word, when the fast-scale oscillations of the inductor current and the capacitor voltage ripple of the converter are periodic. It is therefore necessary to predict fast-scale instability margin for designing the SMC power converters based on Utkin's theory.

In this paper, we apply this concept and design the FFHC controlled tristate DC-DC buck converter for extracting its best optimized performance, i.e, fast transient response without fast-scale instability under wide range of line- and load variation. The paper is organized as follows. Section II revisits the condition of SM in a HDS with single, and multiple switching surfaces. In Section III we describe the proposed system and its mathematical model. We then illustrate how Utkin's equivalent control law and Filippov's method together can be used to design this converter system and to extract its best optimized performance. Finally, in Section V, the performance of proposed scheme is experimentally verified and compared with the classical peak current-mode controlled buck converter without slope compensation.

II. Sliding-Motion in a Discontinuous System

From dynamical system [24], or from control theory point of view [17], the HDSs with right-hand side discontinuity can be descried as

$$\frac{dx}{dt} = f(x) = \begin{cases} f_1(x);\ x \in R_1 & \text{if} \quad h(x) < 0 \\ f_2(x);\ x \in R_2 & \text{if} \quad h(x) > 0 \end{cases} \tag{1}$$

where $R_{1,2}(x) \in \Re^2$ are the smooth regions separated by an one-dimensional discontinuous switching hyper-surface $h(x)$. The systems are called continuous switching if $f_1(x) = f_2(x)$ at any point of the boundary $\Sigma_{1,2}$ separating two adjacent regions R_1 and R_2, and the vector $\dot{x}$ is uniquely defined at any point of the state space and trajectories in region R_1 approaching transversally the boundary $\Sigma_{1,2}$, cross it and enter into the adjacent region R_2. By contrast, in discontinuous systems (called Filippov systems), two different vectors $\dot{x}$, namely $f_1(x)$ and $f_2(x)$, can be associated to a point $x \in \Sigma_{1,2}$. If the transversal components of $f_1(x)$ and $f_2(x)$ have the same sign, the trajectory crosses the boundary and has at that point, a discontinuity in its tangent vector. On the contrary, if the transversal components of $f_1(x)$ and $f_2(x)$ are of opposite sign, i.e., if the two vector fields are pushing in opposite directions, the state of the system is forced to remain on the boundary and slide on it. Although, in principle, motions on the boundary could be defined in different ways [19], the most natural one is Filippov convex method [24] that defines sliding motions on Σ as the solutions on $\Sigma_{1,2}$ of the continuous ordinary differential equation

$$\frac{dx}{dt} = F(x) = \alpha f_1(x) + (1-\alpha) f_2(x) \tag{2}$$

where $F(x)$ is a convex combination of $f_1(x)$ and $f_2(x)$ tangent to $\Sigma_{1,2}$ at x, with a scalar function $\alpha = \frac{\partial h(x)/\partial x f_2(x)}{\partial h(x)/\partial x [f_2(x) - f_1(x)]} \in [0,1]$. Generically, this convex combination is unique. Thus, the state portrait of a Filippov system is composed of the sliding state portrait on Σ defined by boundaries $\Sigma_{1,2} = \{x \in h(x) : \alpha = 0, 1\}$ and of the standard state evolutions in each region $R_{1,2}$ as shown in Fig. 1(a).

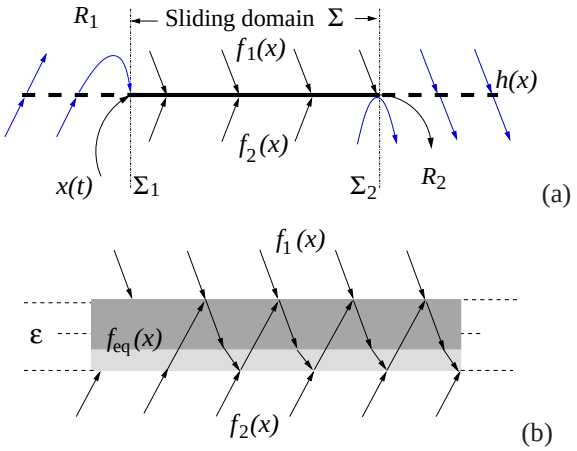

Fig. 1. A representative diagram showing: (a) the direction of both piecewise smooth vector fields $f_1(x)$ and $f_2(x)$ for a sliding motion on an ideal switching surface $h(x)$

happen when the long-time averaged values of coefficients α_1, α_2, and α_3 becomes constant [20], [25]. These coefficients are known as the Fillipov coefficients. Once these coefficient are well defined, there will not be any transversal components of the average vector field $f_{\rm eq}(x) \in (f_1(x), f_2(x), f_3(x))$ along the SS. We can write this transversal condition mathematically as

$$\frac{\partial h(x)}{\partial x} f_{\rm eq}(x) = 0 \tag{4}$$

Here, it is important to note that the equation (4) is inherently same, as the SM determined from the Utkin's equivalent control [17] for single discontinuous SS. Where the dynamics is essentially determined by replacing the discontinuous control input u by an equivalent control $u_{\rm eq}$, given by the solution of $\frac{dh(x)}{dt} = 0$, or $\frac{\partial h(x)}{\partial x} f_{\rm eq}(x, u_{\rm eq}) = 0$, if such a solution exists. When the state-space dynamic is expressed in the form $\frac{dx}{dt} = Ax + Bu + D$, the equivalent control may be explicitly calculated by

$$u_{\rm eq} = -\left[\frac{\partial h(x)}{\partial x} B\right]^{-1} \frac{\partial h(x)}{\partial x}[Ax + D], \tag{5}$$

where $\frac{\partial h(x)}{\partial x} B$ should be a nonsingular square matrix. Substituting (8) into (7), we get the equivalent dynamics

$$\dot{x} = Ax - B\left[\frac{\partial h(x)}{\partial x} B\right]^{-1} \frac{\partial h(x)}{\partial x}[Ax + D]. \tag{6}$$

Therefore a solution is an absolutely continuous vector-valued function, which outside the surfaces satisfies (1), and on and inside their boundaries satisfies (6) for almost all t, as mentioned before.

III. Modeling of FFHC Controlled DC-DC Buck Converter

The schematic diagram of a FFHC controlled tristate buck converter is shown in Fig. 2(a). It consists of an inductor L, a capacitor C, a load resistance R, a conduction loss series resistance r, an uncontrollable switch D, and two controllable switches Q_1 and Q_2. The switching of the Q_1 and Q_2 are controlled by the FFHC control logic.

A. Controller Architecture and Switching Logic

The controller architecture to achieve such switching logic circuit is implemented by means of a nested feedback controller. The slow outer voltage controller is used to generate the quasi-stationary boundary layers [25] of the hysteresis loop. This is achieved by obtaining the equivalent reference current signals $i^+_{\rm ref}$ and $i^-_{\rm ref}$ as a linear combination of the output capacitor voltage v and a reference voltage $V_{\rm ref}$ in the form

$$i^+_{\rm ref} = k_p(V_{\rm ref} - v), \quad \text{and} \quad i^-_{\rm ref} = i^+_{\rm ref} - \Delta \tag{7}$$

where k_p is the gain of the proportional controller, and Δ is the bandwidth between $i^+_{\rm ref}$ and $i^-_{\rm ref}$. While the fast inner current controller is used to generate the binary control signal $u \in (0, 1)$ where $u = (u_1 \ u_2)^T$, by comparing the sensing inductor current i with two threshold reference currents $i^+_{\rm ref}, i^-_{\rm ref}$ and an externally generated clock pulse of time period T. The

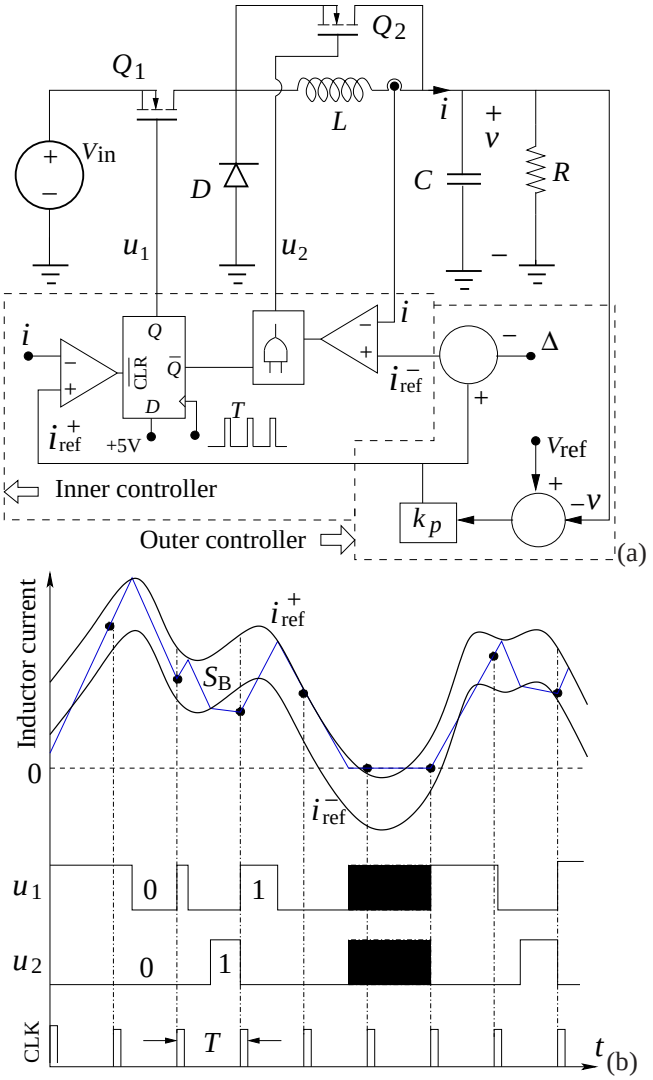

Fig. 2. (a) Schematic diagram of the FFHC controlled tristate buck converter. (b) Generation of binary switching signals u_1 and u_2 in a switching box S_B. Here black region indicates where both switches Q_1 and Q_2 are turned off.

combination of these three signals eventually forms a bounded "chattered box" or simply called the *switching box*

$$S_B = \{(i, v) : i^-_{\rm ref} \le i \le i^+_{\rm ref}, t < T\} \in \Re^2 \tag{8}$$

for this converter system. Depending on the initial position of the inductor current $i(0)$, the converter may operate into two modes: one when the inductor current i is outside the boundary layers and the other when it is inside. At the beginning of the every switching cycles, we determine whether the inductor current $i|_{t=T}$ is within the boundary of S_B or not. If it is inside, at the start of the clock period, the switch Q_1 is turned on and Q_2 is turned off, the inductor current i raise. When i reaches a peak value $i^+_{\rm ref}$, the Q_1 is turned off. The inductor current i starts falling until it reaches the lower threshold current $i^-_{\rm ref}$. The switch Q_2 is turned on when i reaches $i^-_{\rm ref}$ and remains on until the arrival of the next clock pulse. If i reaches next clock pulse with a nonzero value without intersecting $i^-_{\rm ref}$, the operation is said to be in continuous conduction mode

B_1

B_3

of state variables $x(dT) = \begin{bmatrix} V_{\rm ref} - V_o & i^+_{\rm ref} \end{bmatrix}^T$ (V_o represents the steady-state dc output voltage) and solving, the solution of subsystem equation (10), given as

$$x(T) = e^{A_2(1-d)T}x(dT) + \int_{dT}^{T} e^{A_2(T-\tau)}B_2 d\tau;\ \forall x \in M_2 \quad (18)$$

where d is the steady-state duty ratio, the critical inductor current i_c can be easily expressed as a function of on/off switching instants inductor current $i(dT)$. However, since $x(T)$ in (18) is a function of matrix exponent $e^{A(1-d)T}$, one cannot find its exact explicit form of expression as a function of $i(dT)$. Based on first-order approximation, it can expressed

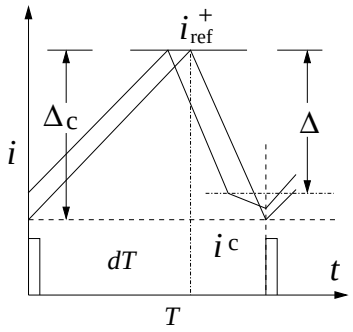

Fig. 5. Inductor current at the edge of CCM operation.

explicitly as

$$i_c = i^+_{\rm ref} - \frac{r(1-d)T}{L}i^+_{\rm ref} - \frac{d(1-d)T}{L}V_{\rm in} \quad (19)$$

where $i(dT) = i^+_{\rm ref}$ and $i^+_{\rm ref}$ is the upper boundary function defined by $i^+_{\rm ref} = k_p(V_{\rm ref} - v)$. Further substitution of $i^+_{\rm ref}|_{t=dT} \approx k_p(V_{\rm ref} - dV_{\rm in})$ into (19) therefore yields the critical condition

$$\Delta_c = \frac{rk_p(1-d)T}{L}V_{\rm ref} + \frac{d(1-d)T(1-rk_p)}{L}V_{\rm in} \quad (20)$$

Here, the parameters r, L, T, $V_{\rm ref}$ are known and others k_p, $V_{\rm in}$ and d are unknown. Keeping $V_{\rm in}$ and all other parameters constant, from (20) we can get the maximum current ripple Δ required for the PCCM operation is at d = 0.5:

$$\Delta = \frac{k_p rT}{2L}V_{\rm ref} + \frac{(1-rk_p)T}{4L}V_{\rm in} \quad (21)$$

For every clock cycle, the value of Δ in (21) thus gives us the necessary condition for a successful converter operation in PCCM when state vectors evolve inside the boundary layers of S_B periodically. In two-dimensional state space, a representative periodic evolution of state trajectories and their corresponding boundary layers are shown in Fig. 6.

However, it is important to note that in each clock cycle, trajectories may evolve outside or inside boundary layers of S_B. For an arbitrary initial position $x(0)$, the controller

$$u = \begin{cases} \left.\begin{array}{ll} u_1^+ = 1, & h_1(x) < 0 \\ u_1^- = 0, & h_1(x) > 0 \end{array}\right\} \text{if } x \text{ is outside} \\ u_{\rm eq} \in (u_1, u_2), \ \text{ if } x \text{ is inside} \end{cases} \quad (22)$$

therefore drives the trajectories to reach into S_B in finite time $t_s > 0$. Once they reach, a hysteretic flow inside the switching box starts and an equivalent motion continue to move toward the quasi-equilibrium point.

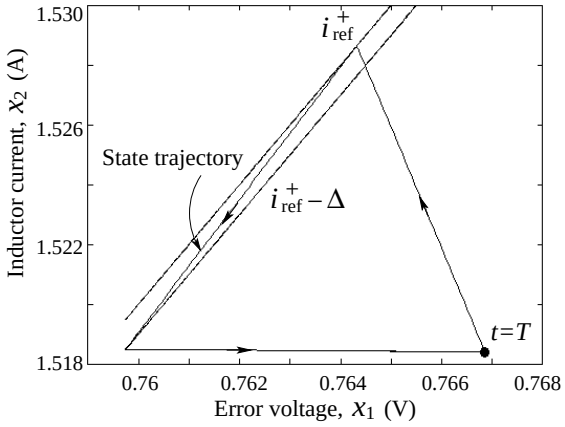

Fig. 6. A typical periodic trajectory evolution of FFHC controlled tristate buck converter within the switching box S_B for L=200μH, C=100μF, r=0.01Ω, Δ=0.001, T=2μs, k=1, k_p=5.5, $V_{\rm ref}$=5V, $V_{\rm in}$=12V, and R=7.5Ω.

IV. SM AND SMC IN THE FFHC CONTROLLED TRISTATE BUCK CONVERTER

The classical smooth equivalent control law (8) always approximates the dynamics due to MSSs. Because of this improper approximation, achieving a unique solution of real power electronic systems is not so straightforward. The systems having single SS or MSSs with $\Delta \to 0$ always have a unique solution [24], [17], whereas in multi-scale power electronics systems, the unique solution only exits when the long-time averaging of *fast-scale* oscillations become zero (as explained in Section II). This zero average dynamics condition, however, can be obtained by analyzing the stability of a periodic orbit. There are four general approaches which are normally used to analyze fast scale instability: 1) the Poincaré map [27], [28]; 2) the Floquet theory; and 3) the monodromy matrix using Filippov theory [29]. To apply this concept, we organize this section as follows. First, based on an ideal switching surface $h(x)$, the conditions for the existence of a sliding mode are found. Second, using monodromy matrix, the fast-scale stability analysis is performed and corresponding regions of different periodic orbits are identified for safe operating condition. Finally the equivalent equation of the motion is derived to design the controller accordingly.

A. Existence Conditions of ϵ-neighborhoods SSs

Assume there exist ϵ-neighborhoods SSs (where $\epsilon \to 0$), given by

$$h(x) = k_p x_1 - k x_2 \quad (23)$$

From Utkin theory [17], we know that a SM exists in the vicinity of a switching surface $h(x)$ if the following local reachability conditions: $\lim_{h(x)\to 0^-} \frac{dh(x)}{dt} > 0$, and $\lim_{h(x)\to 0^+} \frac{dh(x)}{dt} < 0$, or $\lim_{h(x)\to 0} \frac{dh(x)}{dt} h(x) < 0$ are simultaneously satisfied. The explicit form of such ϵ neighborhood reachability condition can be derived by simply substituting the time derivative of $h(x)$

$$\frac{dh(x)}{dt} = \frac{\partial h(x)}{\partial x}\frac{dx}{dt} = \begin{cases} Jf_1(x) > 0 & \text{if} \quad h(x) < 0 \\ Jf_2(x) < 0 & \text{if} \quad h(x) > 0 \end{cases} \quad (24)$$

quasi-periodicity; and limit cycle oscillations [7]. Out of these nonlinear phenomena, there are two degenerate cases — *quasi-periodicity* and *chaos*, where the inductor current i inside S_B can either aperiodically oscillates and hits the corner of S_B [7] or moves without hitting the corner points if it evolves on a torus. The dynamics is then characterized by the existence of two (or more) frequencies which are incommensurate [31], [32] and the duty ratios of the converter would not be well defined. In such situations, the existence conditions (25) and (26) which were originally defined for single SS is not valid always for deriving equivalent control law with MSSs. The representative bifurcation diagram of the FFHC controlled buck converter is shown in Fig. 8 where the sampled inductor current taken as the plotted variable. At high values of R, a stable period-1 orbit exists in PCCM. However, with a decrease in R, this orbit becomes unstable through a smooth period-doubling bifurcation at $R \approx 7.05\Omega$. Subsequently, one of the branches of the period-2 orbit hits the border between PCCM and CCM operation at $R \approx 6.83\Omega$ as shown in Fig. 9(a). Available theory predicts that this bifurcation also leads to and a direct transition from a periodic orbit to aperiodic orbit. As the parameter is further reduced, a series of smooth and border collision bifurcations occur in close succession, and finally it bifurcates into a chaotic behaviors at $R \approx 4.68\Omega$. The continuous-time waveform of a typical chaotic inductor current oscillation at $R = 4\Omega$ is shown in Fig. 9(b).

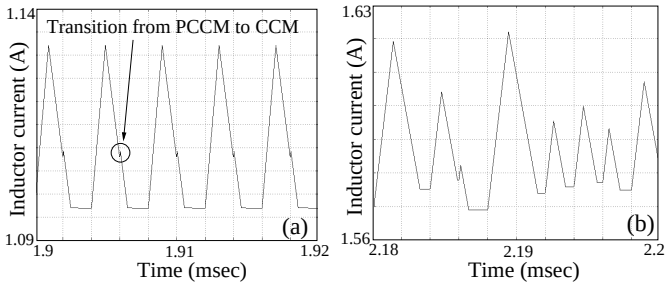

Fig. 9. The continuous-time inductor current waveform showing: (a) the direct transition from PCCM to CCM operation for R=6.83Ω, and (b) a typical chaotic oscillation for R=4.68Ω.

Thus, we can see that, if the converter operates in PCCM, the existence conditions (25) and (26) derived for a ϵ-neighborhood of $h(x)$ can be successfully used only for a guaranteed reaching condition of trajectories into S_B, but not for the SM of that hysteretic flow inside.

B. Existence Region for Hysteretic Flow

In order to identify existence region of the high frequency hysteretic flow inside and to observe the stability status of the converter system, it is therefore necessary to estimate the fast-scale stability margin at the clock speed [23]. It is also required to estimate the range of external parameters that will ensure periodic operation without the onset of chaos. The sampled-data model (or Poincaré map) addressed earlier [27], [6] to solve this problem. Even though it is conceptually simple, it yields complicated equations for most converters, and as a result, this approach has not found widespread acceptance among mainstream power electronic practitioners. The stability analysis using the fundamental solution matrix over a complete cycle or monodromy matrix, thus provides an alternative method of obtaining the Jacobian of the Poincaré map when the nonlinear map cannot be explicitly derived.

The monodromy matrix is eventually a composition of the state transition matrices for the pieces of the orbit that lie in the individual subsystems, and the saltation matrix can be expressed as [24], [33]

$$S = I + \frac{[f^+(x) - f^-(x)]\partial h(x)/\partial x}{\partial h(x)/\partial x\, f^-(x) + \partial h(x)/\partial t} \tag{28}$$

where I is the identity matrix of the same order as the number of state variables. When converter operates in PCCM, the state transition matrix over the complete cycle can be then composed of the state transition matrices over the three phases of evolution and three saltation matrices for the switching from M_1 to $M_2(S_1)$, from M_2 to the free-wheeling state $M_3(S_2)$ and finally switching back to $M_1(S_3)$ [34]:

$$W = S_3\Phi_3 S_2\Phi_2 S_1\Phi_1 \tag{29}$$

where the state transition matrices Φ_1, Φ_2 and Φ_3 are obtained as matrix exponentials $e^{A_1 d_1 T}$, $e^{A_2 d_2 T}$ and $e^{A_3 d_3 T}$ respectively. In order to evaluate these, one needs to know the duty ratio d_1, d_2, and d_3. This can be obtained following [27] using the Newton-Raphson method. Alternatively one can use any standard simulator to obtain the stable behavior, from which the information about d_1, d_2, and d_3 can be extracted. In calculating the saltation matrix S_1, the switching function is $h_1(x) = k_p x_1 - k x_2$, so that the normal is $\partial h_1(x)/\partial x = [k_p \;\; -k]$ and the time derivative is $\partial h_1(x)/\partial t = 0$. Similarly, for calculating S_2, the expression for the switching function is simply derived from (19) as $h_2(x) = kx_2 - (k_p x_1 - \Delta)$. Thus $\partial h_2(x)/\partial x = [-k_p \quad k]$ and $\partial h_2(x)/\partial t = 0$. With these expressions, we can obtain the saltation matrices

$$S_1 = I + \frac{(f_2^+ - f_1^-)\dfrac{\partial h_1(x)}{\partial x}}{\dfrac{\partial h_1(x)}{\partial x} f_1^- + \dfrac{\partial h_1(x)}{\partial t}},\; S_2 = I + \frac{(f_3^+ - f_2^-)\dfrac{\partial h_2(x)}{\partial x}}{\dfrac{\partial h_2(x)}{\partial x} f_2^- + \dfrac{\partial h_2(x)}{\partial t}}$$

which are evaluated as

$$S_1 = \begin{bmatrix} 1 & 0 \\ -k_p a_1 & 1 + k a_1 \end{bmatrix},\; S_2 = \begin{bmatrix} 1 - k_p a_2 & k a_2 \\ -k_p a_3 & 1 + k a_3 \end{bmatrix} \tag{30}$$

where

$$a_1 = \frac{V_{\text{in}}/L}{\left(\frac{k_p}{RC} + \frac{k}{L}\right) V_{\text{ref}} - \frac{k}{L} V_{\text{in}} - \left(\frac{k_p}{RC} + \frac{k}{L}\right) x_1 + \left(\frac{rk}{L} - \frac{k_p}{C}\right) x_2}$$

$$a_2 = \frac{x_2/C}{\left(\frac{k_p}{RC} + \frac{k}{L}\right) x_1 - \left(\frac{k_p}{RC} + \frac{k}{L}\right) V_{\text{ref}} - \left(\frac{rk}{L} - \frac{k_p}{C}\right) x_2}$$

$$a_3 = \frac{(V_{\text{ref}} - x_1)/L}{\left(\frac{k_p}{RC} + \frac{k}{L}\right) x_1 - \left(\frac{k_p}{RC} + \frac{k}{L}\right) V_{\text{ref}} - \left(\frac{rk}{L} - \frac{k_p}{C}\right) x_2}$$

and S_3 is an identity matrix. Note that the form of the monodromy matrix is sufficiently general. If the orbit contains passage through more number of subsystems with a number of crossings (for example, in a higher periodic orbit), one

$f_1($

$u_{1\epsilon}$

sur

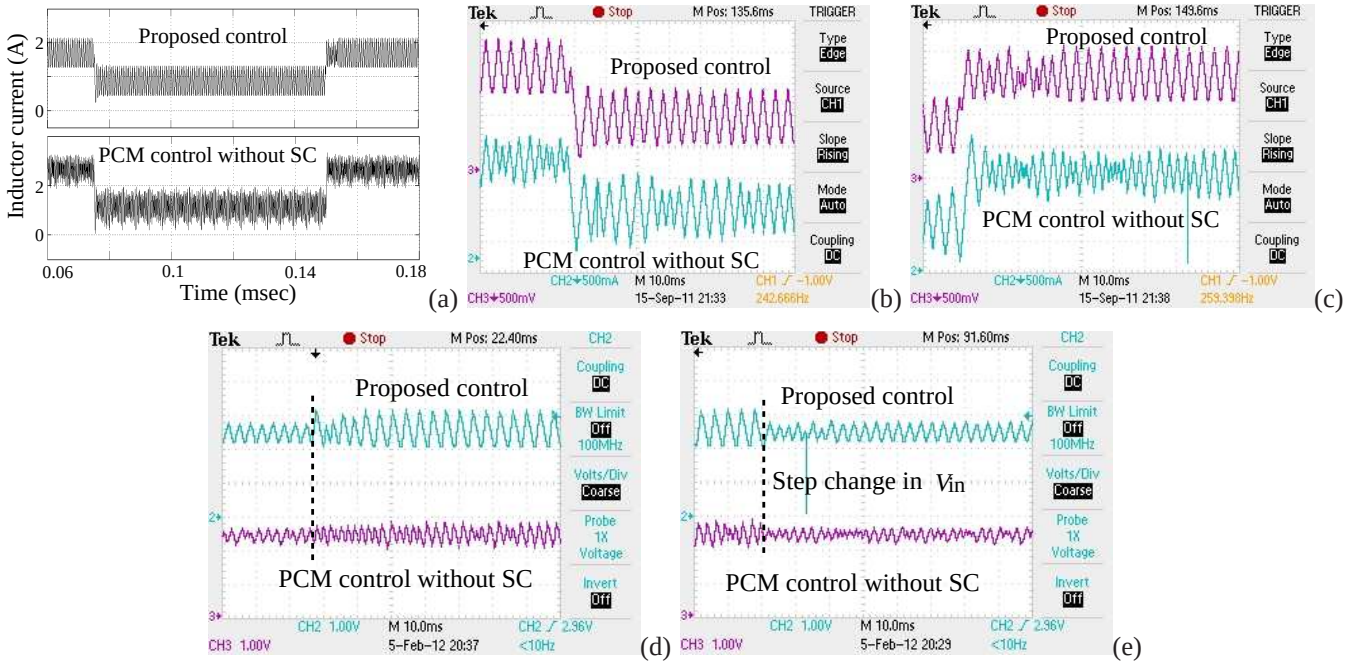

Fig. 13. Comparison of (a) simulation, and experimental inductor current waveforms between proposed FFHC controlled tristate buck converter and conventional PCM controlled buck converter without SC under (b) step load change 3Ω to 6Ω; and (c) 6Ω to 3Ω, and input voltage change (d) 8V to 14V, and (e) 14V to 8V respectively. Here, simulated results show the inductor current response due to change of step load resistance from 3Ω to 6Ω and back to 3Ω.

properties, and the selection of the control parameters are discussed. It is shown that equivalent control based SMC design is only valid when the converter operates in periodic mode. We have also addressed how both Filippov's method and Utkin's equivalent control law together can be used to design, and to extract its best optimized performance. Finally, its performance is experimentally verified and compared with PCM controlled buck converter (without SC). The results demonstrate that, over a wide range of operating conditions (i.e., wide variation of input voltage and load resistance) the transient response of FFHC controller is as good as the reference one, without any subharmonic oscillations. It can be therefore concluded that the proposed FFHC controller may be a good alternative over conventional PCM (without SC) controller to achieve the optimized performance with a low implementation cost and circuit complexity. However, investigations on efficiency and losses calculation under different loading conditions of such controlled system are still necessary. Currently we are working on that.

APPENDIX

To obtain the Jacobian matrix of (33), let us consider $g_1 = \frac{(V_{\rm ref}-x_1)}{RC} - \frac{(x_2-I_0)}{C}$ and $g_2 = \frac{-2(V_{\rm ref}-x_1)(x_2-I_0)}{u_{1\rm eq}T[V_{\rm in}-(V_{\rm ref}-x_1)]} + \frac{V_{\rm in}}{L}u_{1\rm eq}$ where equivalent control input $u_{1\rm eq}$ can be derived by using (5) when $h(x) = h_1(x)$. By substituting the result into (33) and applying $dh_1(x)/dt = 0$, it can be obtained from 9)-(10) as

$$u_{1\rm eq} = \frac{\left(\frac{k_p}{RC}+\frac{k}{L}\right)(V_{\rm ref}-x_1) - \frac{k_p}{C}x_2}{kV_{\rm in}/L}. \qquad (35)$$

Then the linearization of (33) around the equilibrium points $(V_{\rm ref}-V,\ I,\ U_{1\rm eq})$ can be expressed as

$$\frac{d\tilde{x}}{dt} = \begin{pmatrix} \frac{\partial g_1}{\partial x_1} & \frac{\partial g_1}{\partial x_2} \\ \frac{\partial g_2}{\partial x_1} & \frac{\partial g_2}{\partial x_2} \end{pmatrix}\tilde{x} + \begin{pmatrix} \frac{\partial g_1}{\partial u_{1\rm eq}} \\ \frac{\partial g_2}{\partial u_{1\rm eq}} \end{pmatrix}\begin{pmatrix} \frac{\partial u_{1\rm eq}}{\partial x_1} & \frac{\partial u_{1\rm eq}}{\partial x_2} \end{pmatrix}^T \tilde{x} = \begin{pmatrix} J_{11} & J_{12} \\ J_{21} & J_{22} \end{pmatrix}\tilde{x}$$

where

$$\begin{aligned} \frac{\partial g_1}{\partial x_1} &= -\frac{1}{RC}, \frac{\partial g_1}{\partial x_2} = -\frac{1}{C}, \frac{\partial g_2}{\partial x_1} = \frac{2(I-I_{\rm o})V_{\rm in}}{U_{1\rm eq}T(V_{\rm in}-V)^2}, \\ \frac{\partial g_2}{\partial x_2} &= \frac{-2V}{U_{1\rm eq}T(V_{\rm in}-V)}, \frac{\partial g_1}{\partial u_{1\rm eq}} = 0, \\ \frac{\partial g_2}{\partial u_{1\rm eq}} &= \frac{V_{\rm in}}{L} + \frac{2V(I-I_{\rm o})}{U_{1\rm eq}^2T(V_{\rm in}-V)}, \frac{\partial u_{1\rm eq}}{\partial x_1} = \beta_1, \frac{\partial u_{1\rm eq}}{\partial x_2} = \beta_2. \end{aligned}$$

Here $\beta_1 = -\frac{k_p/RC + k/L}{kV_{\rm in}/L}$ and $\beta_2 = -\frac{k_p/C}{kV_{\rm in}/L}$. Substituting these values into above equation, we get

$$\begin{aligned} J_{11} &= -\frac{1}{RC}\ ,\ \ J_{12} = -\frac{1}{C} \\ J_{21} &= \frac{\beta_1 V_{\rm in}}{L} + \frac{2(I-I_{\rm o})V_{\rm in}}{U_{1\rm eq}T(V_{\rm in}-V)^2} + \frac{2\beta_1 V(I-I_{\rm o})}{U_{1\rm eq}^2T(V_{\rm in}-V)} \\ J_{22} &= \frac{\beta_2 V_{\rm in}}{L} - \frac{2V}{U_{1\rm eq}T(V_{\rm in}-V)} + \frac{2\beta_2 V(I-I_{\rm o})}{U_{1\rm eq}^2T(V_{\rm in}-V)} \end{aligned}$$

REFERENCES

[1] "International Technology Roadmap for Semiconductor," 2003. [Online]. Available: http:// www. public.itrs.net

[2] M. T. Zhang, M. M. Jovanovic, and F. C. Lee, "Design considerations for low-voltage on-board DC-DC modules for next generations of data processing circuits," *IEEE Transactions on Power Electronics*, vol. 11, no. 2, pp. 328–337, March 1996.